Vol. 19, No. 2 (2020) 731-744
Revista Mexicana de Ingeniería Química

Effects of agitation rates over metastable zone width (MSZW) of concentration for cane sugar crystallization

Efectos de la velocidad de agitación en la amplitud de la zona metaestable (MSZW) de concentración para la cristalización de azúcar de caña

K.B. Sánchez-Sánchez[1]*, E. Bolaños-Reynoso[2], J.M. Méndez-Contreras[2], R. Cerecero-Enriquez[2]

[1]*Departamento de Ingeniería Química, Tecnológico Nacional de México/I.T. Celaya. Av. Tecnológico y García Cubas s/n. 38010 Celaya, Guanajuato, México.*

[2]*División de Estudios de Posgrado e Investigación, Tecnológico Nacional de México/I.T. Orizaba. Avenida Oriente 9 Núm. 852, 94320 Orizaba, Veracruz, México.*

Received: August 28, 2019; Accepted: October 4, 2019

Abstract

The aim of this work is the experimental measurement of metastable zone width (MSZW) of concentration for sugar cane solutions by means of the polythermal method coupled with an image acquisition system, taking into account the effects of agitation rate and temperature, which represents a key novelty, since this is the first work that considers both variables experimentally. A split plot experimental design was followed with two factors, temperature with four levels (40, 50, 60 and 70 °C), and agitation rate with 3 levels (150, 250 and 350 rpm); the response variables were density (as a measure of concentration) and crystal size distribution. The results allow to demonstrate that agitation rate does not exhibit a statistical effect on the MSZW for the crystallization of cane sugar, attributing the formation of nuclei and their growth to effects by changes in the temperature. This contributes to better understanding of the phenomenological behavior occurring in sugar cane crystallization.

Keywords: MSZW, agitation rate, crystallization, sugar cane, concentration.

Resumen

El objetivo de este trabajo es la medición experimental de la amplitud de la zona metaestable (MSZW) de concentración para soluciones de caña de azúcar mediante el método politérmico junto con un sistema de adquisición de imágenes, teniendo en cuenta los efectos de la velocidad de agitación y la temperatura, lo que representa una novedad clave, ya que esta es el primer trabajo que considera ambas variables experimentalmente. Se siguió un diseño experimental de parcelas divididas con dos factores, temperatura con cuatro niveles (40, 50, 60 y 70 ° C) y velocidad de agitación con 3 niveles (150, 250 y 350 rpm); las variables de respuesta fueron la densidad (como medida de concentración) y la distribución del tamaño de los cristales. Los resultados permiten demostrar que la velocidad de agitación no exhibe un efecto estadístico en la MSZW de concentración para la cristalización de azúcar de caña, atribuyéndose la formación de núcleos y su crecimiento únicamente a efectos por cambios en la temperatura. Esto contribuye a una mejor comprensión del comportamiento fenomenológico que ocurre en la cristalización del azúcar de caña.

Palabras clave: MSZW, velocidad de agitación, cristalización, azúcar de caña, concentración.

1 Introduction

Batch crystallization is a key unit operation for the most effective methods of producing chemicals, pharmaceuticals, agrochemicals, biochemicals, petrochemicals and nutrients (Hojjati *et al*., 2007; Aamir *et al*., 2010; Kalbasenka *et al*., 2011; Nagy and Aamir 2012). This is often the multiproduct plant operating mode, with low volume production capacity and high value end products (Hu *et al*., 2005; Binev *et al*., 2015), it also offers several advantages over other separation techniques such as low operating costs, high purity products in a simple stage and attractive end products for commercial purposes.

Batch crystallization products (crystals) must meet stringent quality requirements, which are determined by the crystal size distribution (CSD), which is measured by the average diameter in % volume (D(4,3)) of the crystal and its standard deviation in % volume (S(4,3)).

* *Corresponding author. E-mail*: kelvyn.baruc@gmail.com
Tel. (+52) 272-139-71-54
https://doi.org/10.24275/rmiq/Proc809
issn-e: 2395-8472

These properties are directly affected by some aspects of operation such as the seeding time and its characteristic CSD, the agitation rate (Kim *et al*., 2002; Kalbasenka *et al*., 2004; Akrap *et al*., 2010; Ni and Liao, 2010; Sander *et al*., 2012, Chianese and Kramer, 2012; Bolaños *et al*., 2014), the imposed cooling trajectory (Bolaños, 2000; Bolaños *et al*., 2008), and the supersaturation profile (Xiaobo *et al*., 2009).

Generally, the cane sugar crystallization operation focuses on the supersaturation (Sr) control, known as the driving force for the nucleation and growth (Hojjati *et al*., 2007). Operating the crystallizer at high supersaturation results in the production of large number of nuclei that compete with the seeds and reduce the overall crystal size (D(4,3)). Also, it makes the downstream separation stages more difficult. In the opposite case, operating the crystallizer close to the saturation limits decrease the crystal growth rate, followed by a decrease in the economical process feasibility. Known the above implications related to the solution supersaturation, it is important to define an optimal operation zone, called metastable zone width (MSZW) of concentration to increase the performance of the crystallization operation. The MSZW is defined as the supersaturation level where spontaneous nucleation is generated. It is specified by two temperature values, the first one (lower), determined by the saturation temperature and the upper one, determined by the temperature at which the first crystals are detected (Kadam *et al*., 2012).

Most operating strategies are based on the implementation of temperature profiles as a function of time in order to maintain the concentration within the first metastable zone. The temperature profiles are calculated based on the use of trial and error experimentation (Quintana *et al*., 2004; Bolaños *et al*., 2008), mathematical modelling (Quintana *et al*., 2008; Nagy *et al*., 2008; Mesbah *et al*., 2010; Myronchuk *et al*., 2013) and in the direct design approach (Fujiwara *et al*., 2005; Sarkar *et al*., 2006; Nagy *et al*., 2009; Bolaños *et al*., 2018). However, recently Bolaños *et al*., (2014) reported that the agitation rate significantly influences the growth dynamics of the crystal, modifying its CSD through the process time. Therefore, the experimental knowledge of MSZW of concentration behavior at different levels in agitation rate is essential to ensure that the process is always within the desired metastable zone, considering temperature and agitation rate in its prediction.

The aim of this work is the experimental measurement of MSZW of concentration for sugar cane solutions by means of the polythermal method (Sangwal, 2011) coupled with an image acquisition system (Bolaños *et al*., 2008; Bolaños et al, 2014), taking into account the effects of agitation rate and temperature, which represents a key novelty, since this is the first work that use both variables experimentally. The results will yield better understanding of the phenomenological behavior occurring in sugar cane crystallization, and improve the operation conditions at industrial crystallization, allowing to specify optimal operating trajectories, increasing the overall process performance to achieve strict requirements in the final product quality and reducing environmental impact.

2 Scientific background

Akrap *et al*., (2010), studied the effect of agitation speed on the metastable zone amplitude, supersaturation level, crystal growth and crystal size distribution of borax decahydrate. They concluded that the parameters mentioned above are significantly influenced by the hydrodynamic regime in the system.
Velázquez *et al*., (2010), evaluated for the first time experimentally the limits of the concentration zones for refined cane sugar in terms of density. They obtained the mathematical models that describe these zones by analyzing CSD, micrograph sequences and growth kinetics.
Wong *et al*., (2011), carried out a study to refine the lines that delimit the zones of concentration for α-lactose monohydrate, using electronic microscopy for the detection of the first visible nucleus. They reported that the temperature and concentration of appearance of the first visible nucleus was independent of the agitation rate. In contrast, the agitation rate had significant effects on the amplitude of the nucleation zone, increasing as the agitation rate increased.
Frawley *et al*., (2012), studied the effect of agitation rate on nucleation and supersaturation. It was observed that for higher agitation rate there is a larger area of glass for solute deposition which promotes accelerated crystal growth. They used the moment's method to solve the population balance.
Sander *et al*., (2012), observed that the conditions of the process of obtaining pentaerythritol by batch cooling crystallization influence the CSD. They determined that an optimum cooling profile, lower retention time, higher agitation rate and lower seed surface area improved the CSD.

Kaćunić *et al*., (2013), conducted a detailed study on the effect and position of the agitator on the crystallization of borax decahydrate, presenting as a result that both factors affect the supersaturation of the solution. In addition, the shape of the crystals at the end of the batch is also affected, since each type of agitator has different regimes within the crystallizer, so that the crystals suffers attrition in its contours.

Bolaños *et al*., (2014), studied the effects of agitation rate on the average diameter (% of volume D (4.3)) in the cane sugar batch crystallization at pilot-scale process. The mathematical model presented includes the population balance equation (EBP), the mass and energy, and the equations of the kinetics of nucleation and growth. They found that agitation rate modifies the dynamic behavior of crystal growth but not the formation of crystal mass.

Sánchez *et al*., (2017), presented an operating condition analysis for the cane sugar crystallization process, both pilot and industrial scale, with a MSZW approach coupled to the solutions of mechanistic kinetic models (thermodynamic models). The MSZW of concentration was used as a strategy to limit the temperature and concentration within the saturation and metastable curves. The study allows to analyses different industrial operating strategies to compare its performance at the macroscopic level to the pilot-scale plant.

3 Materials and methods

3.1 Experimental set-up

The equipment used for the experimental stage was a batch glass crystallizer stirred tank with heating jacket, isolated with fiberglass, equipped with an electronic system for regulating the agitation rate and thermocouples type J for temperature measurement and registration. The crystallizer is installed in a metal structure secured to the ground to avoid vibrations that affect the structure of the equipment and generate noise in the measurements.

The crystallizer has a programmable recirculation bath JULABO model F34, agitation motor coupled to an Allen-Brabdley frequency inverter for the regulation of agitation rate and an image acquisition system through a microscope and a high-resolution digital camera. The high-precision DMA-4500 (Anton Paar) digital densimeter was used to measure the concentration (density in g/cm^3), which bases its measurement on the harmonic oscillation method of U-tube, with measurement range from 0 to 3 g/cm^3, sample feed of 1 ml, temperature measurement error of 0.1 °C and 1x10^{-5} g/cm^3 for density error, with sampling time of 5 minutes. Table 1 presents the detailed experimental set-up.

Table 1. Detailed device of batch crystallizer set-up.

Quantity	Device
1	Glass crystallizer 6 L, heating-cooling jacket 2.55 L crystallizer dimensions: height 35 cm and internal diameter of 14.4 cm, lower dome height of 1.8 cm.
1	Generic variable speed motor, direct transmission from 0 to 1.500 rpm, 60 Herz, 127 VAC and 760 W, stirring arrow 14 in (length) and 1/4 of diameter with 316 stainless steel.
1	Impeller of 4 rectangular rings with 90 ° of separation between each crossing. Blades with 2 in length and 1 in width. 316 stainless steel.
2	Thermocouple J type. 0 to 760 ºC, wire-rope, 3m.
1	Programmable recirculating bath Julabo F-34 with temperature range of - 34 at 200 °C, with recirculation pump 15 L/min, bath volume of 14-20 L, 120 VAC / 60 Hz.
1	Densimeter DMA-4500 Anton-Paar, measurement range of 0-3 g/cm^3, measurement error in the temperature 0.1 °C and 1x10^{-5} g/cm^3 in density. Serial port connection RS-232.
1	Professional microscope: Carl Zeiss, model 37081, Primo Star iLED.
1	Digital microscope camera AxioCam ERc5S. CMOS sensor. USB connectivity and HDMI.
1	Programmable tachometer. Range from 50 - 999,999 rpm.
1	Optical sensor for distances of 3 ft. Range 1 - 150,000 rpm.
1	PC Intel QuadCore, 4 Gb RAM.

3.2 Image acquisition system

The polythermal method is based on the appearance and detection of the first nuclei while the solution is cooled at a constant rate (Sangwal, 2011). For the analysis of the first visible nuclei and the crystals, an image acquisition system was used, which consists of capturing micrographs taken with an AxioCam ERc5S digital microscope camera, coupled to a 4-objective microscope and through the use of AxioVision Rel. 4.8.2 software by Carl Zeiss Vision. It should be noted that the objective used was the Plan - ACHROMAT10x / 0.25.

The methodology for the acquisition of micrographs is as follows:

1 A liquid sample (5 mL) is taken using a hose and deposited on a slide, previously heated at the same samples' temperature.

2 10 images of crystals from different parts of the sample are taken using a 10X magnification

3 Carry out an automated measurement of the areas (nuclei) by using the algorithm reported by Sánchez (2018), which comprises an advanced image segmentation procedure, capable to identify conglomerates of particles (nuclei or crystals) with high precision.

4 Perform the conversion of pixels (px) to microns (μm) using a conversion factor calculated with an improved Neubauer chamber. In this work, the value was 1 px equals 1.045 μm.

5 Compute the CSD, in terms of average diameter in % volume D(4.3) and its corresponding standard deviation S(4.3) by using the data from the previous step.

It is important to note that this technique has been experimentally validated by Córdova (2004) against average diameters in % volume D(4.3) in a specialized Malvern Instruments MasterSizer 2000 equipment. In addition, Bolaños *et al*., (2008) and Bolaños *et al*., (2014) have successfully applied it. To perform steps 4 and 5 in an automated way, the CSD.jl software was used (Sánchez and Bolaños, 2019), written in Julia Language Programming (Bezanson *et al*., 2015).

3.3 MSZW of concentration measurement

To measurement the MSZW of concentration, a split plot experimental design (DoE) was followed, where two factors were considered, temperature with four levels (40, 50, 60 and 70 ° C), and agitation rate with 3 levels (150, 250 and 350 rpm), with the temperature as the randomized factor; the response variables were density (as a measure of concentration) and crystal size distribution (CSD). The DoE were performed in duplicate with a total of 24 experiments.

The MSZW of concentration of sugar solutions were measured using the polythermal method reported by Akrap *et al*. (2010) and Sangwal (2011), which is applied as follow: saturated solutions of commercial cane sugar (high purity) at different equilibrium temperatures (40, 50, 60 and 70 ºC) were prepared in a cooling batch crystallizer (see details in Table 1). Table 2 presents the details and quantities for each saturated solution for the 4 levels of temperature. The established weight of each solution was 4500 g (g sugar/mL water), so that the sampling was not an importance variable to consider and to be able to handle the system as constant volume.

The dissolution process was carried out by recirculation of heating water in the jacket, with a temperature of 10 °C higher than the saturation temperature of the solution (40, 50, 60 and 70 °C), until a complete dissolution solution was obtained, this was verified through the microscope to observe that there were no crystals within the solution. Once the solution reached the saturation concentration without crystals, according with experimental solubility curve expressed in Eq. (1) (temperature range: 40 °C - 70 °C) (Velázquez *et al*., 2010), the solution was cooled down at a given linear cooling rate in intervals of 1 ºC.

Table 2. Quantities used for each saturated solution.

Temperature of saturation (°C)	Weight of solution (g sugar / mL water)	Mass of sugar (g)	Volume of water (mL)
70	4500	3440.83	1059.17
60	4500	3334.97	1165.03
50	4500	3220.32	1279.68
40	4500	3096.91	1403.09

For each temperature stationary state, a solution sample (5 mL) was taken to measure the concentration (density (g/cm^3)) using a densimeter model DMA 4500 Anton Paar and capture images in the AxioCam ERc5S digital microscope camera. In order to cool down the solution, a Julabo F-34 brand recirculation bath was used, which was controlled from the central computer of the process through an RS-232 communication port.

$$\rho_{sat} = 1.28522 + 0.00146 * T - 5.7875 * 10^{-6} * T^2 \quad (1)$$

To quantify the limits of MSZW of concentration, the images were analyzed for the identification of the first visible nucleus, providing the temperature and density where the limit of the growth zone is located. Subsequently, the experimental areas of the formed nuclei were obtained and the appearance of agglomerates and the dispersion of the CSD was quantified by the software CSD.jl (Sánchez and Bolaños, 2019). Finally, a statistical analysis of the experimental data was performed in order to quantify the effect of temperature, agitation rate and its interaction on the amplitude of the concentration zones.

4 Results and discussion

4.1 Concentration analysis based on cooling temperatures and agitation rate

Figure 1 shows a sequence of representative images describing each metastable zone of concentration. In Figure 1a, the saturated solution is free of crystals, meaning that the concentration is within the first metastable zone. Next, Figure 1b shows the appearance of the first visible nuclei, representing the second metastable zone. Finally, the appearance of agglomerates in Figure 1c gives the end for the second metastable zone, and the beginning of the labile zone.

Defining the limit for the second and labile zone is complicated, and the CSD analysis should be taken in consideration. Is worth mentioning that special care was taken to keep the sample at the same temperature to prevent the sudden formation of nuclei in the process of measurement of concentration and CSD.

Figure 2 presents experimental density for each saturation temperature (40, 50, 60 and 70 °C) and agitation rate (150, 250 and 350 rpm); R1 and R2 correspond to both experiments performed. An average of 10 samples were taken for each run, as described in Section 3. Density shows a uniform behavior for all saturation temperatures. Special care was taken to avoid the presence of formed crystals, or remnants of the solution stage in saturated solutions before starting the experimental run. Also, it was sought to start the run when the density was as close as possible to the solubility curve, for this purpose the solubility curve corrected by Velázquez *et al*., (2010) was considered.

It is observed that the densities for each saturation temperature and agitation rate tend to increase as the temperature decreases, confirming that by decreasing the temperature the density is increased, causing the system to find thermodynamic equilibrium by generating crystallization. Despite this, certain points are also observed where the density decreases, this may be due to the fact that as the solution is concentrated and the temperature decreases, nuclei are formed and growing having an opposite effect, that is, the density decreases due to the presence mass transfer to the faces of the formed nuclei.

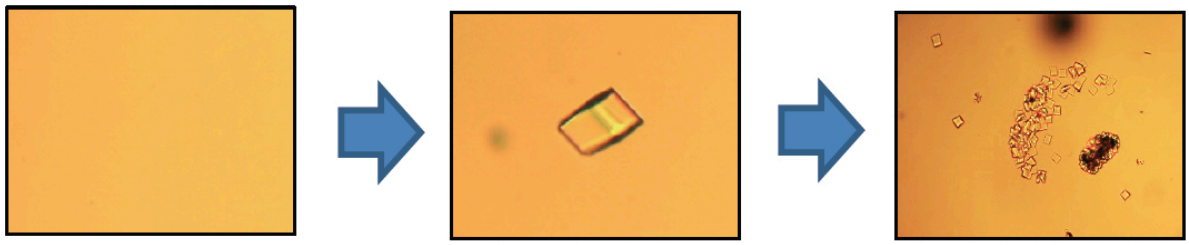

Fig. 1. MSZW identification, a) First metastable zone, b) Second metastable zone and c) Labile zone.

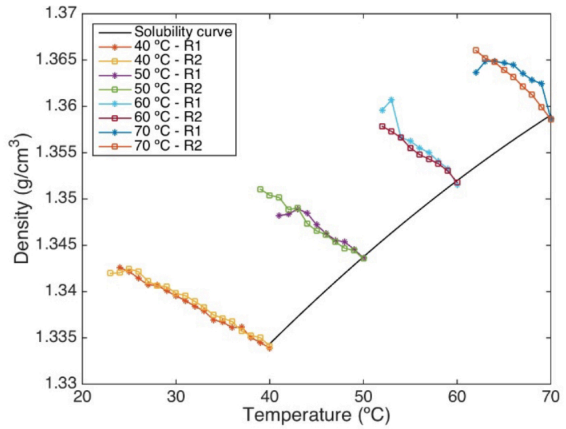

a)

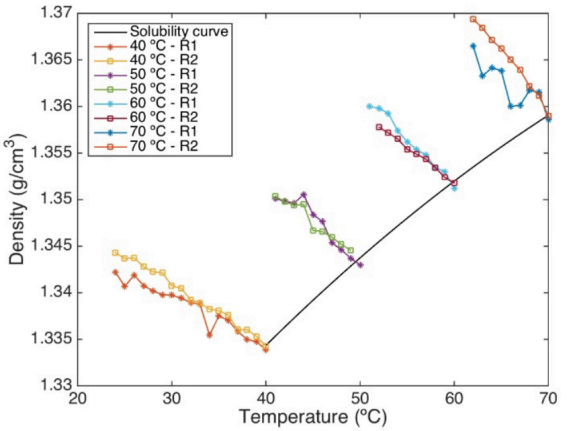

b)

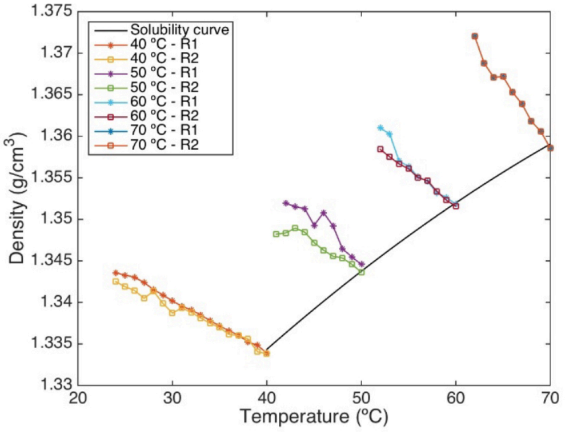

a)

Fig. 2. Experimental data for temperature vs density: a) 150 rpm, b) 250 rpm and c) 350 rpm.

On average, for the saturated solution at 40 °C a cooling temperature range of 40 to 23 °C and density of 1.33340 to 134275 g/cm^3, for 50 °C a cooling temperature range of 50 to 39 °C and density of 1.34367 to 1.34984 g/cm^3, for 60 °C a cooling temperature range of 60 to 51 °C and density of 1.35161 at 1.35949 g/cm^3 and for 70 °C a cooling temperature range of 70 to 62 °C and density of 1.35867 to 1.36828 g/cm^3. These ranges of concentration and temperature are essential for the determination of the concentration limits (critical points) of the metastable and labile zones, complementing the determination of the latter with the measurements and analysis of the CSD.

4.2 CSD analysis

Figs. 3-5 show the CSD in % volume for each saturated solution (40, 50, 60 and 70 °C) and agitation rate (150, 250 and 350 rpm), respectively. These Figs., in combination with the analysis of the micrographs for the appearance of agglomerates, allow to determine the location of the labile line.

In the CSD graphs (Figs. 3-5), when the % volume drops suddenly, crystallization can be considered to be located in the labile zone, and therefore allows the amplitude of the metastable nucleation zone to be specified.

In Figure 3a, which represents the experimental run starting at 40 °C and 150 rpm, the appearance of nuclei at the temperature of 26 °C is identified with D(4,3) = 31.1061 μm and S(4,3) = 5.7581 μm, to end with 24 °C with a D(4,3) = 33.1400 μm and S(4,3) = 7.4673 μm. The change in the % volume between temperatures of 27 °C and 26 °C is noticeable, where the % volume goes from 28 to 19, this temperature point and its corresponding experimental density represent a critical point for the labile line. Subsequently, in Figure 3b, which represents the experimental run starting at 50 °C and 150 rpm, nuclei at the temperature of 47 °C are identified with a D(4,3) = 57.9968 μm and S(4,3) = 1.5293 μm, to end with 24 °C with a D(4,3) = 54.4697 μm and S(4,3) = 18.6679 μm. Here the sudden change in the % volume is between the temperatures of 46 °C and 45 °C, where the % volume goes from 52 to 18, represents the critical point for the labile line.

In Figure 4a, which represents the experimental run starting at 40 °C and 250 rpm, the appearance of nuclei at the temperature of 26 °C is identified with a D(4,3) = 32.0897 μm and S(4,3) = 8.6513 μm, to end with 24 °C with D(4,3) = 100.6491 μm and S(4,3) = 34.9226 μm. Again, it is simple to observe the temperature point (26 °C) where the % volume drop exists to identify the critical point of the labile line.

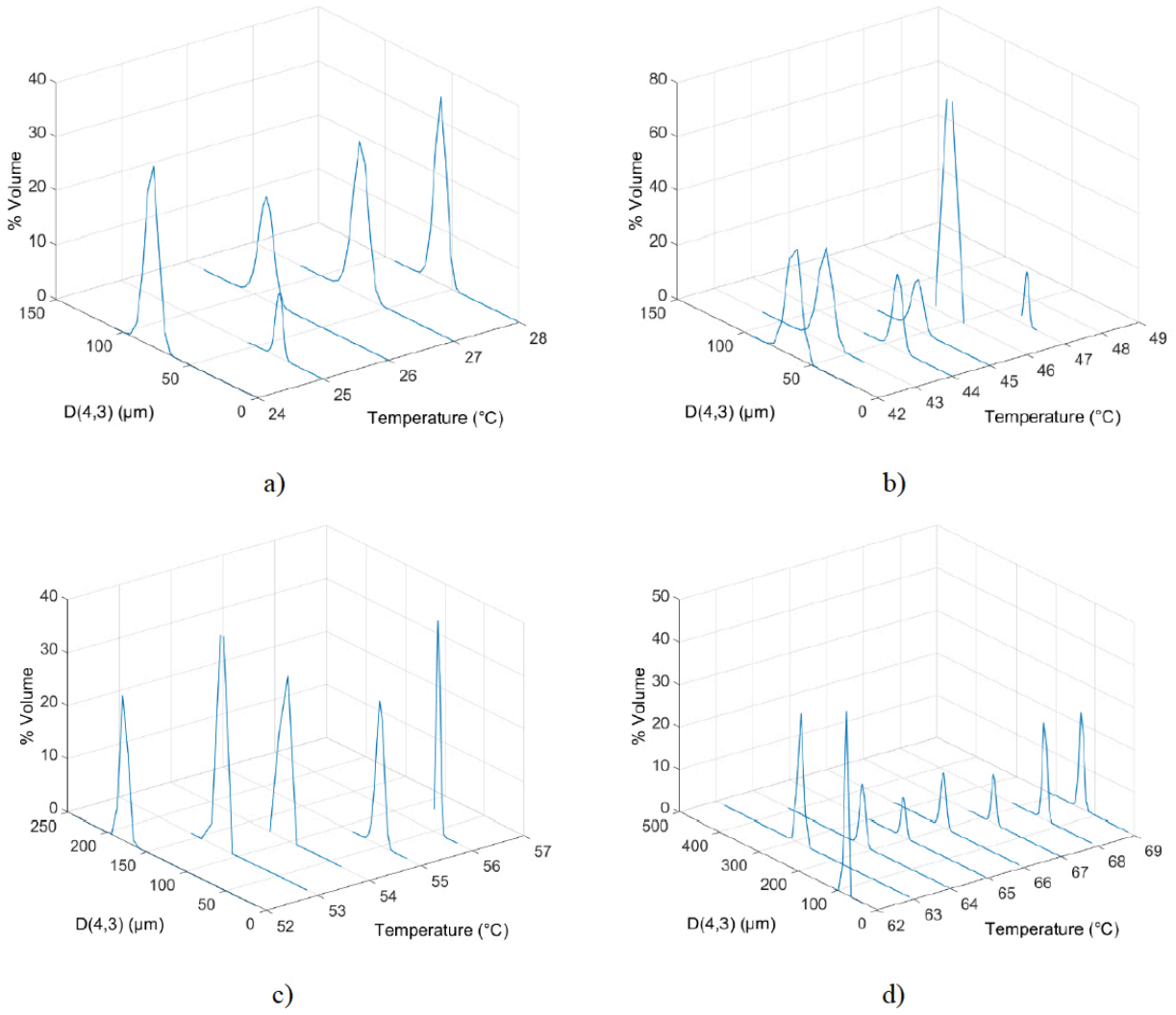

Fig. 3. CSD in % volume at 150 rpm for saturation temperature of: a) 40 °C, b) 50 °C, c) 60 °C and d) 70 °C.

Finally, in Figure 5b, which represents the experimental run starting at 50 °C and 350 rpm, the appearance of nuclei at the temperature of 47 °C is identified with D(4,3) = 48.7765 μm and S(4,3) = 15.5444 μm, to finish with 44 °C with a D(4,3) = 43.2112 μm and S(4,3) = 10.3921 μm. In this case, the change in % volume occurred up to 44 °C. Similarly, for Figure 5d the critical point is located at 67 °C.

CSD analysis is a useful tool for identifying the state of the crystals through temperature variation. However, and as can be seen in Figure 4c, some cases the % volume increases considerably when the temperature decreases. This can be attributed to the lack of crystals in the micrographs taken at these temperatures, which makes the CSD tend to give greater weight to larger crystals, dramatically increasing the % volume, making identification of the critical point difficult. To overcome this situation, visual analysis should be used to identify a sudden presence of agglomerates, which also represents the critical point for the labile line.

To exemplify this phenomenon, an image sequence of 70 to 62 °C (150 rpm) is presented in Figure 6, where it is possible to appreciate the evolution of the appearance of nuclei, their growth and formation of agglomerates (critical point for the labile line), to later observe the identification of crystals larger in size that have grown within the saturated solution.

Table 3. Quantities used for each saturated solution.

			Saturated solution at 40 °C		Saturated solution at 50 °C		Saturated solution at 60 °C		Saturated solution at 70 °C	
		Agitation rate (rpm)	Temp. (ºC)	Dens. (g/cm^3)	Temp. (ºC)	Dens. (g/cm^3)	Temp. (ºC)	Dens. (g/cm^3)	Temp. (ºC)	Dens. (g/cm^3)
Intermediate	line	150	27.5	1.3409	47	1.3455	56.5	1.3549	69	1.3612
		250	30	1.3401	46	1.3471	58	1.3534	68.5	1.3618
		350	31	1.3395	47	1.3474	57.5	1.3543	68	1.3618
Labile	line	150	26	1.3417	44.5	1.3476	54.5	1.356	67.5	1.3625
		250	27.5	1.342	44	1.35	56.5	1.3548	66.5	1.3626
		350	29	1.3408	45.5	1.349	55.5	1.3557	67	1.3639

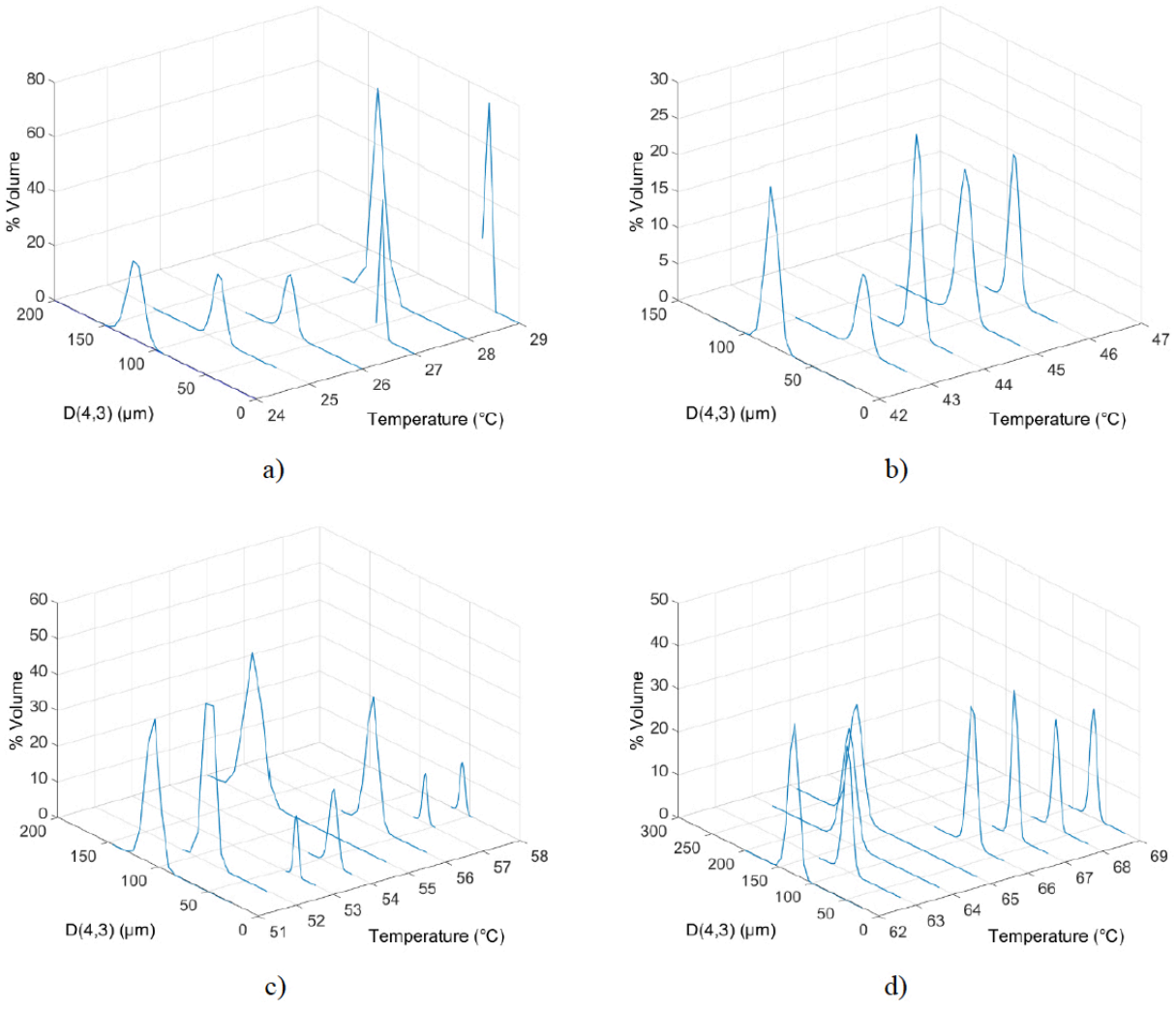

Fig. 4. CSD in % volume at 250 rpm for saturation temperature of: a) 40 °C, b) 50 °C, c) 60 °C and d) 70 °C.

4.3 MSZW of concentration

Table 3 shows the critical concentration - temperature points identified from the CSD analysis (Section 4.2) for intermediate and labile lines in terms of density for each saturation temperature and agitation rate. A non-linear fitting (Levenberg-Marquardt algorithm) was applied to the experimental data, obtaining Eqs. (2) - (4), modelling the intermediate line of the metastable zone, and Eqs. (5) - (7) modelling the labile line. Eqs. (2) - (7) can be used over a temperature range of 40 °C - 70 °C.

Intermediate line at 150 rpm with $R^2 = 0.9652$:

$$\rho_{int.150} = 1.342 - 0.0002087 \cdot T + 7.47E-06 \cdot T^2 \quad (2)$$

Intermediate line at 250 rpm with $R^2 = 0.9986$:

$$\rho_{int.250} = 1.337 - 9.672E-05 \cdot T + 6.64E-06 \cdot T^2 \quad (3)$$

Intermediate line at 350 rpm with $R^2 = 0.9999$:

$$\rho_{int.350} = 1.331 + 0.000119 \cdot T + 4.909E-06 \cdot T^2 \quad (4)$$

where ρ_{int} is the density in the intermediate line of the metastable zone in g/cm^3. For a temperature range of 70 to 40 °C, the density range of the $\rho_{int.150}$ model is 1.33610 to 1.34461 g/cm^3, the $\rho_{int.250}$ model is 1.36277 to 1.34376 g/cm^3 and the $\rho_{int.350}$ model is 1.336338 to 1.34361 g/cm^3 respectively.

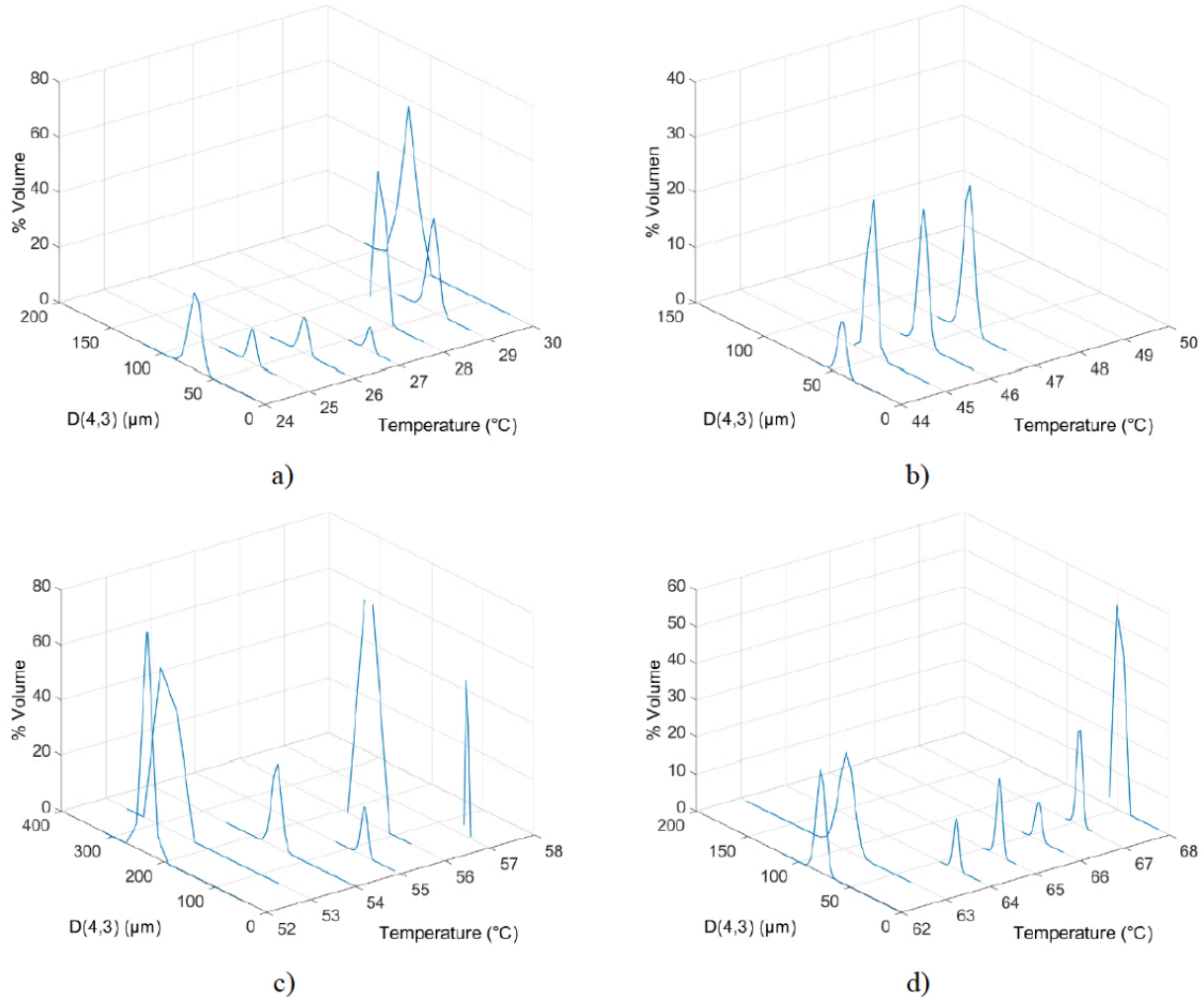

Fig. 5. CSD in % volume at 350 rpm for saturation temperature of: a) 40 °C, b) 50 °C, c) 60 °C and d) 70 °C.

Labile line at 150 rpm with $R^2 = 0.9810$:

$$\rho_{labil.150} = 1.336 + 6.835E - 0.5 \cdot T + 4.802E - 06 \cdot T^2 \quad (5)$$

Labile line at 250 rpm with $R^2 = 0.9908$:

$$\rho_{labil.250} = 1.335 + 0.0001389 \cdot T + 3.954E - 06 \cdot T^2 \quad (6)$$

Labile line at 350 rpm with $R^2 = 0.9998$:

$$\rho_{labil.350} = 1.332 + 0.0001492 \cdot T + 4.79E - 06 \cdot T^2 \quad (7)$$

where ρ_{labil} is the density of labile line in g/cm^3. For a temperature range of 70 to 40 °C the density range of the $\rho_{labil.150}$ model is 1,36431 to 1,34642 g/cm^3, the $\rho_{labil.250}$ model is 1,36410 to 1,34688 g/cm^3 and the $\rho_{labil.350}$ model is 1,36592 to 1,34563 g/cm^3, respectively.

For the 6 models obtained, satisfactory adjustments (R^2) are presented, all of them exceeding 95%. This establishes that the second order polynomial model is suitable for the adjustment of the experimental data obtained, with good correlation. With these adjusted models, the concentration vs temperature diagram was plotted (see Figure 7), in order to observe the variability present in the amplitude of the concentration zones produced by the effects of agitation rate.

As a result, intermediate and labile lines described by the polynomial models are located within a nearby region, overlapping in the majority of the temperature range (45-70 °C). There is no clear and significant effect of the agitation rate on the amplitude of the concentration zones.

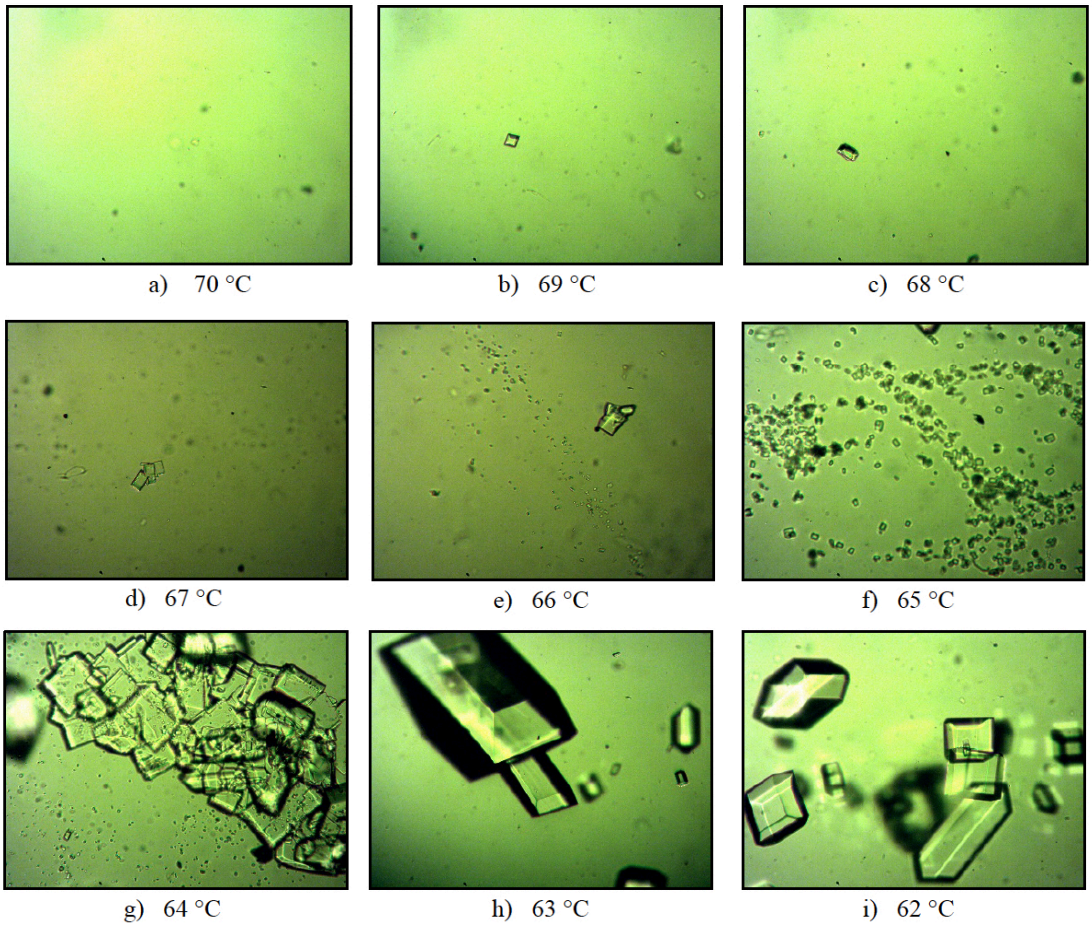

Fig. 6. Image sequence of crystal formation and growth for saturated solution at 70 ° C and 150 rpm.

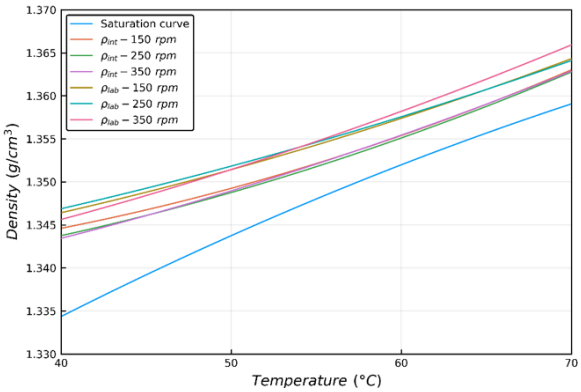

Fig. 7. MZSW of concentration for sugar cane crystallization.

In the case of the intermediate line, the 3 fitted models (Eqs. 2 - 4) have the same trend, start and end at similar density values (1.34399 - 1.36050 g/cm^3), and in the complete range of temperature, it is not possible to identify a trend of the effect of the agitation rate. In the case of the labile line, the corresponding model for an agitation rate of 350 rpm has a slight positive deviation (0.12%) with respect to the 150 and 250 rpm models. Similarly, no significant variability is observed.

The above described behavior differs of reported by Akrap *et al*., (2010) and also Sander *et al*. (2012) for borax decahydrate and pentaerythritol, respectively, where the effect of the agitation rate was extremely significant. This can be attributed to the fact that each solute used in crystallization has different organic properties and exhibits different crystallization phenomena (Chianese and Kramer, 2012). According to Quintana *et al*. (2008) and Bolaños *et al*. (2014), sugar cane crystallization has a nucleation order of 6.27E-04 - 5.00E-02, while pentaerythritol has 6.25 - 32.5 (Chianese *et al*., 1995; Cheon *et al*., 2005), this significant difference in nucleation order reflects that nucleation rate in sugar cane is mainly promoted by supersaturation (low parameter value), while for pentaerythritol could be due to supersaturation (high parameter value) and agitation rate. In the case of agitation rate, Bolaños *et al*. (2014) reported parameter p = 1.41 (agitation rate parameter) for sugar cane which is greater than the nucleation order, supporting that MSZW for sugar cane crystallization is mainly affected by supersaturation. It is important to remark that kinetic parameters for borax decahydrate and pentaerythritol related to agitation rate are not available.

Another important factor that should be considered is the crystallizer geometry and the type of agitator (Kaćunić *et al*., 2013), where Akrap *et al*., (2010) used an agitator with 4 flat blades and Sander *et al*., (2012) an axial flow impeller with 4 inclined vanes. This is due to the fact that different types of agitators generate different regimes within the solution, modifying the viscosity, increasing or decreasing the crystal-agitator collisions, etc., as reported by Akrap *et al*., (2010).

The results are comparable to those reported by Velázquez *et al*., (2010), where the same concentration zones were identified for the same solute. These data show a deviation of 0.11% against those obtained in this work, which present temperature and density data lower than those reported in the literature. This may be due to Velázquez *et al*., (2010) used a 4X objective, and an image size of 640 x 480 px (highest resolution available in the publication date), which makes it impossible to observe small nuclei. On the other hand, in this work a microscope of higher image resolution was used (see Table 1) with a 10X objective and 1280 x 960 px image size, which allowed to analyze in detail each sample in search of nuclei.

4.4 Statistical analysis

A statistical analysis was carried out applied to the split plot experimental design for MSZW of concentration limits: intermediate and labile. For the intermediate limit, p-values were 0.0000, 0.9701 and 0.2799 for temperature (T), agitation rate (AR) and interaction of T-AR, respectively. The low p-value (0.0000) for the temperature indicates a high significant effect on the amplitude of concentration zones (MSZW). This result is expected because the experiments were carried out at different temperatures, which affects the density during crystallization of sugar cane. The agitation rate factor (AR) (p-value of 0.9701) and interaction (T-AR) (p-value of 0.2799) have no statistical effect (p-value > 0.05). In the case of the labile line, p-values were 0.0000, 0.9079 and 0.2605 for temperature (T), agitation rate (AR) and interaction of T-AR, respectively. Again, agitation rate factor (AR) and interaction (T-AR) have no statistical effect (p-value > 0.05). This study allows to demonstrate that agitation rate has not a defined effect on the MSZW of concentration for sugar solutions. Therefore, these statistical analyses confirm the presented results in Section 4.4

Conclusions

Agitation rate has a high impact on CSD, due to mechanical interactions with the impeller, crystallizer geometry, and viscosity. However, this study allows to demonstrate that agitation rate does not exhibit a phenomenological and statistical effect on the MSZW of concentration for sugar solutions (sugar cane - water) for both, intermediate and labile limits (lines). Therefore, selection of an optimal agitation rate is independent of MSZW of concentration and should be based from their influence upon other variables such as the CSD.

The empirical models presented can be used with great precision to track the evolution of concentration in the sugar cane crystallization process. They differ from the reported previously in literature due to the use of high-resolution image acquisition system and better algorithm (automated) to quantify particles in images.

References

Aamir, E., Nagy, Z. K., Rielly, C. D. (2010). Evaluation of the effect of seed preparation method on the product crystal size distribution for batch cooling crystallization processes. *Crystal Growth & Design 1*, 4728-4740. https://doi.org/10.1021/cg100305w

Akrap, M., Kuzmanic, N., Kardum, P. J. (2010). Effect of mixing on the crystal size distribution of borax decahydrate in batch cooling crystallizer. *Journal of Crystal Growth 312*, 3603-3608. https://doi.org/10.1016/j.jcrysgro.2010.09.023

Bezanson, J., Edelman, A., Karpinski, S., Shah, V. B. (2015) Julia: A fresh approach to numerical computing. arXiv:1411.1607v4

Binev, D., Seidel-Morgenstern, A., Lorenz, H. (2015). Study of crystal size distributions in a fluidized bed crystallizer. *Chemical Engineering Science 133*, 116-124. https://doi.org/10.1016/j.ces.2014.12.041

Bolaños, R. E., Sánchez, S. K. B., Urrea, G. G. R., Ricardez, S. L. A. (2014). Dynamic Modeling and Optimization of Batch Crystallization of Sugar Cane under Uncertainty. *Industrial & Engineering Chemistry Research 53*, 13180-13194. https://doi.org/10.1021/ie501800j

Bolaños, R. E. (2000). Control and optimization of operating conditions from cooling batch crystallizers. Ph. D. Thesis. I.T. de Celaya, México.

Bolaños, R. E., Xaca, X. O., Álvarez, R. J., López, Z. L. (2008). Effect analysis from dynamic regulation of vacuum pressure in an adiabatic batch crystallizer using data and image acquisition. *Industrial & Engineering Chemistry Research 47*, 9426-9436. https://doi.org/10.1021/ie071594i

Bolaños, R. E., Sánchez, S. K. B., López, Z. L., Ricárdez, S. L. (2018). A study on empirical and mechanistic approaches for modelling cane sugar crystallization. *Revista Mexicana de Ingeniería Química 17*, 389-406. https://doi.org/10.24275/10.24275/uam/izt/dcbi/revmexingquim/2018v17n2/Bolanos

Cheon, Y. H., Kim, K. J., Kim, S. H. (2005). A study on crystallization kinetics of pentaerythritol in a batch cooling crystallizer. *Chemical Engineering Science 60*, 4791-4802. https://doi.org/10.1016/j.ces.2005.03.035

Chianese, A., Kramer, M. J. H. (2012). *Industrial Crystallization Process Monitoring and Control*. Wiley-VCH. https://doi.org/10.1002/9783527645206

Chianese, A., Karel, M., Mazzarotta, B. (1995). Nucleation kinetics of pentaerythritol. *The Chemical Engineering Journal 58*, 209-214. https://doi.org/10.1016/0923-0467(94)02896-6

Córdova P. N. M. (2004). Determination of the seed conditions to maximize the growth of particles obtained by batch cooling crystallization. Master Thesis, Instituto Tecnológico de Orizaba. Orizaba, Veracruz, México.

Frawley, J. P., Mitchell, A. N., Ó'Ciardhá, T. C., Hutton, W. K. (2012). The effects of supersaturation, temperature, agitation and seed surface on the secondary nucleation of paracetamol in ethanol solutions. *Chemical Engineering Science 75*, 183-197. https://doi.org/10.1016/j.ces.2012.03.041

Fujiwara, M.; Nagy, Z. K.; Chew, J. W.; Braatz, R. D. (2005). First- principles and direct design approaches for the control of pharmaceutical crystallization. *Journal Process Control 15*, 493-504. https://doi.org/10.1016/j.jprocont.2004.08.003

Hojjati, H., Sheikhzadeh, M., Rohani S. (2007). Control of supersaturation in a semibatch antisolvent crystallization process using a fuzzy logic controller. *Industrial & Engineering Chemistry Research 46*, 1232-1240. https://doi.org/10.1021/ie060967x

Hu, Q., Rohani, S., Jutan, A. (2005). Modelling and optimization of seeded batch crystallizers. *Computers & Chemical Engineering 29*, 911-918. https://doi.org/10.1016/j.compchemeng.2004.09.011

Kaćunić, A., Akrap, M., Kuzmanić, N. (2013). Effect of impeller type and position in a batch cooling crystallizer on the growth of borax decahydrate crystals. *Chemical Engineering Research and Design 91*, 274-285. https://doi.org/10.1016/j.cherd.2012.07.010

Kadam, S. S., Kulkarni, S. A., Coloma Ribera, R., Stankiewicz, A. I., ter Horts, J. H., Kramer, H. J. M. (2012). A new view on the metastable zone width during cooling crystallization. *Chemical Engineering Science 72*, 10-19. https://doi.org/10.1016/j.ces.2012.01.002

Kalbasenka, A., Huesman, A., Kramer, H. (2011). Modeling batch crystallization processes: Assumption verification and improvement of the parameter estimation quality through empirical experiment design. *Chemical Engineering Science 66*, 4867-4877. https://doi.org/10.1016/j.ces.2011.06.049

Kalbasenka, A., Huesman, A., Kramer, H. (2004). Impeller frequency as a process actuator in suspension crystallization of inorganic salts from aqueous solutions. In: *11th International Workshop on Industrial Crystallization*. 135-143.

Kim, Y. H., Lee, K., Koo, K. K., Shul, Y. G., Haam, S. (2002). Comparison study of mixing effect on batch cooling crystallization of 3-Nitro-1,2,4-triazol-5-one (NTO) using mechanical stirrer and ultrasound irradiation. *Crystal Research & Technology 37*, 928-944. https://doi.org/10.1002/1521-4079(200209)37:9<928::AID-CRAT928>3.0.CO;2-R

Mesbah, A., Landlust, J., Huesman, A. E. M., Kramer, H. J. M., Jansen, P. J., Van den Hof, P. M. J. (2010). A model-based control framework for industrial batch crystallization processes. *Chemical Engineering Research and Design 88*, 1223-1233. https://doi.org/10.1016/j.cherd.2009.09.010

Myronchuk, V., Yeshchenko, O., Samilyk, M. (2013). Sucrose cooling crystallization modelling. *Journal of Faculty of Food Engineering 12*, 109-114. http://www.fia.usv.ro/fiajournal/index.php/FENS/article/view/150/148

Nagy, Z. K. (2009). Model based robust control approach for batch crystallization product design. *Computers & Chemical Engineering 33*, 1685- 1691. https://doi.org/10.1016/j.compchemeng.2009.04.012

Nagy, Z., Aamir, E. (2012). Systematic design of supersaturation controlled crystallization processes for shaping the crystal size distribution using an analytical estimator. *Chemical Engineering Science 84*, 656-670. https://doi.org/10.1016/j.ces.2012.08.048

Nagy, Z. K.; Fujiwara, M.; Braatz, R. D. (2008). Modelling and control of combined cooling and antisolvent crystallization processes. *Journal of Process Control 18*, 856-864. https://doi.org/10.1016/j.jprocont.2008.06.002

Ni, X., Liao, A. (2010). Effects of mixing, seeding, material of baffles and final temperature on solution crystallization of L-glutamic acid in an oscillatory baffled crystallizer. *Chemical Engineering Journal 156*, 226-233. https://doi.org/10.1016/j.cej.2009.10.045

Quintana, H. P., Bolaños, R. E., Miranda, C.B., Salcedo, E. L. (2004). Mathematical modeling and kinetic parameter estimation in batch crystallization. *AIChE Journal 50*, 1407-1417. https://doi.org/10.1002/aic.10133

Quintana, H. P. A., Uribe, Martínez. B., Rico, R. V., Bolaños, R. E. (2008). Comparative analysis of power low type and diffusion-integration

kinetic equations in batch cooling of sugar cane. *Revista Mexicana de Ingeniería Química 7*, 171-182. http://rmiq.org/iqfvp/Pdfs/Vol%207%20no%202/RMIQ_9.pdf

Sánchez, S. K. B. (2018). Optimization of operating conditions for the batch crystallization of sugar cane through the implementation of programmed trajectories in MSZW and image processing. PhD Thesis, I. T. de Orizaba, México.

Sánchez, S. K. B., & Bolaños, R. E. (2019, August 27). Kelvyn88/CSD.jl: RMIQ Paper Release (Version v1.1). *Zenodo*. http://doi.org/10.5281/zenodo.3379085

Sánchez, S. K. B., Bolaños, R. E., Urrea, G. G. R. (2017). Analysis of operating conditions for cane sugar batch crystallization based on MSZW coupled with mechanistic kinetic models. *Revista Mexicana de Ingeniería Química 16*, 1031-1054. http://rmiq.org/iqfvp/Pdfs/Vol.%2016,%20No.%203/Sim2/Sim2.html

Sander, A., Kardum, P. (2012). Pentaerythritol crystallization. Influence of the process conditions on the granulometric properties of crystals. *Advanced Powder Technology 23*, 191-198. https://doi.org/10.1016/j.apt.2011.02.001

Sangwal, K. (2011). Recent developments in understanding of the metastable zone width if different solute-solvent systems. *Journal of Crystal Growth 318*, 103-109. https://doi.org/10.1016/j.jcrysgro.2010.11.078

Sarkar, D., Rohani, S., Jutan, A. (2006). Multi-objective optimization of seeded batch crystallization processes. *Chemical Engineering Science 61*, 5282-5295. https://doi.org/10.1016/j.ces.2006.03.055

Xiaobo, S., Xianghaim L., Yu, W., Guoji, L. (2009). Measurement and correlation of solubilities of adipic acid in different solvents. *Chinese Journal of Chemical Engineering 17*, 473-477. https://doi.org/10.1016/S1004-9541(08)60233-5

Velázquez, C. O., Bolaños, R. E., Lopez, Z. L., Alvarez, R. J. (2010). Experimental evaluation of the concentration zone widths in cane sugar crystallization using data and image acquisition. In: *Proceedings of the World Congress on Engineering*, London, U. K. http://www.iaeng.org/publication/WCE2010/WCE2010_pp709-714.pdf

Wong, S. Y., Bund, R. K., Connelly, R. K., Hartel, R. W. (2011). Determination of the dynamic metastable limit for α-lactose monohydrate crystallization. *International Diary Journal 21*, 839-847. https://doi.org/10.1016/j.idairyj.2011.05.003